https://doi.org/10.2352/EI.2024.36.17.AVM-107

Evaluation of Signal and Noise Metrics of High Dynamic Range Image Sensors by IEEE P2020 Methodology

Orit Skorka[1], Paul Romanczyk[2], Jackson Knappen[2], Norman Koren[2], Jonathan Phillips[2], and Radu Ispasoiu[1]
[1] onsemi, San Jose, CA, USA; [2] Imatest, Boulder, CO, USA

Abstract

Quantification of the image sensor signal and noise is essential to derive key image quality performance indicators. Image sensors in automotive cameras are predominately activated in high dynamic range (HDR) mode, however, legacy procedures to quantify image sensor noise were optimized for operation in standard dynamic range mode. This work discusses the theoretical background and the workflow of the photon-transfer curve (PTC) test. Afterwards, it presents example implementations of the PTC test and its derivatives according to legacy procedures and according to procedures that were optimized for image sensors in HDR mode.

Introduction

Key image quality performance indicators of electronic image sensors are derived from signal and noise parameters of raw image data. Legacy procedures to quantify noise were historically written at a time when image sensors were mostly operated in standard dynamic range (SDR) mode, in which signal saturation is limited by the photodetector full well capacity (FWC). These days, activation of image sensors in high dynamic range (HDR) mode is widespread, especially in applications where brightness levels of the scene span an extremely broad range, such as with automotive cameras. In HDR mode, there is a mechanism that enables extension of signal saturation to a level that is significantly higher than the FWC. Common methods that are used at present to achieve HDR response are multi-exposure [2], lateral overflow integration capacitor (LOFIC) [3], and split photodiode [4].

Figure 1. *Photo of a HDR scene as captured with a demo camera that included an automotive image sensor which was activated in HDR mode.*

Sensor dynamic range (DR) is defined as the ratio between its saturation signal and its noise equivalent signal. In SDR mode, a typical DR is 70 dB. In HDR mode, a typical DR is 120 dB, and these days, there are image sensors with DR that exceeds 140 dB. **Figure 1** presents a photo of an outdoor scene as captured with a demo camera with an automotive image sensor in HDR mode.

While legacy procedures for signal and noise characterization, such as the ones detailed in the EMVA 1288 standard [1], are easy to implement with image sensors in SDR mode, they can be difficult or impractical to implement with image sensors in HDR mode. IEEE P2020 is a Standards Association working group meant to address attributes relating to image quality of automotive imaging systems. The IEEE P2020 Noise Standard aims to define test procedures that are optimized for present day automotive image sensors, including considerations for HDR modes.

Photon-Transfer Curve

The photon-transfer curve (PTC) test allows for derivation of important image sensor parameters through analysis of signal and noise properties from image sets in raw data format that are captured under varied exposure conditions [5].

Noise in CMOS Image Sensors

In electronic imaging, noise is defined as the unwanted variations in the digital output of the system. The total noise has a temporal component and a fixed-pattern component. Temporal noise, σ_{temp}, represents signal fluctuations over time under constant illumination, and fixed-pattern noise (FPN), σ_{FPN}, represents mean signal variations in a uniformly illuminated pixel region.

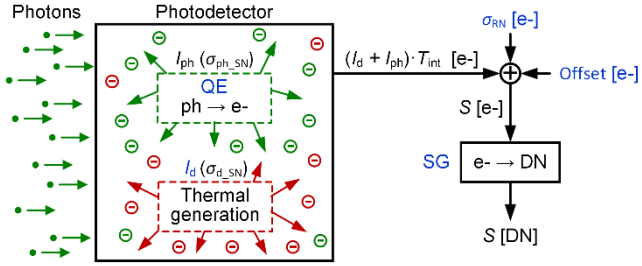

Figure 2. *A simplified model of a pixel in a CMOS image sensor to illustrate signal components, sources of temporal noise, and the signal path.*

There are three sources of temporal noise in the pixel signal of CMOS image sensors (CIS); they are explained using the simplified pixel diagram in **Figure 2**. The first is the dark-current shot noise, σ_{d_SN}. This noise is associated with the thermal generation process in the photodetector, which produces the dark current, I_d, and it has Poisson statistics. The second is the photon shot noise, σ_{ph_SN}. This noise, which also has Poisson statistics, is associated with the photo generation process in the photodetector. Photo generation, which produces the photo current, I_{ph}, depends on the quantum efficiency (QE). The immediate photodetector signal at the end of integration time, T_{int}, is $(I_d + I_{ph})\cdot T_{int}$. When this signal travels in the readout chain [6], it collects read noise, σ_{RN}, and a time invariant offset

signal. Read noise is the third source of temporal noise; it is originated by the readout chain.

At the end of the path, the total pixel signal, S, is converted from charge into digital numbers (DN) with a conversion factor that is called the system gain (SG). For simplicity, the model skips conversion of charge into voltage and voltage into DN. In the diagram, the mean I_d, the photodetector QE, the mean σ_{RN}, the offset signal, and the SG, are pixel parameters that vary among pixels in the array.

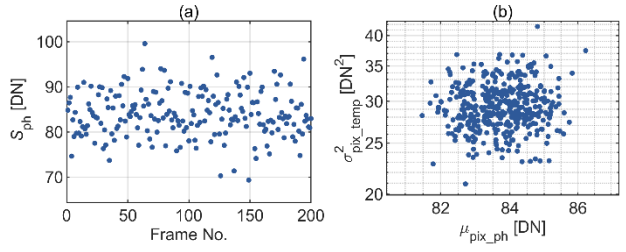

Figure 3. Results from repeated simulation of S_{ph} of: (a) A 3 µm pixel under constant illumination when Tj = 60 °C. (b) An array of 20×20 pixels under the same simulation conditions as in (a) with small variations in pixel parameters.

Figure 3 (a) presents results from simulation of a 3 µm pixel at 60 °C junction temperature, T_j, under constant illumination with 530 nm light, T_{int} = 33 ms, and low gain. The simulation was repeated 200 times, and the photo signal, S_{ph} was calculated by subtraction of the mean pixel dark signal, μ_{pix_d}, from S at each frame. Signal fluctuations are caused by temporal noise. The mean and standard deviation of this data set are the pixel mean photo signal, μ_{pix_ph}, and the pixel temporal noise, σ_{pix_temp}, respectively, under the selected simulation conditions.

Although all pixels in an image sensor are fabricated at the same time with the same process, they are not completely identical. To demonstrate the effect of variations in pixel parameters on statistical properties, **Figure 3** (b) presents $\sigma^2_{pix\_temp}$ versus μ_{pix_ph} results from simulation of 20×20 pixels that are similar to the one from **Figure 3** (a) with small variations in pixel parameters that followed a normal distribution model. Simulation conditions were the same as in **Figure 3** (a), and the simulation was repeated 200 times for each pixel. The variation in μ_{pix_ph} is the σ_{FPN} of this group of pixels under the selected simulation conditions.

Simulated and Measured PTC Plots

Figure 4 (a) and (b) present results from simulation of the same 20×20 pixels when illumination was varied. Like before, the simulation was repeated 200 times for each pixel at each illumination level. Each group of data points with the same color represents results for the same mean illumination level, which is expressed in photons-per-pixel units. **Figure 4** (c) presents a summary plot, where μ_{ph} and σ^2_{FPN} are mean and variance of μ_{pix_ph} at each illumination level in **Figure 4** (a), respectively, and σ^2_{temp} is the mean of $\sigma^2_{pix\_temp}$ in **Figure 4** (b). μ_{ph} can also be calculated by subtraction of the mean dark signal, μ_d, from the mean total signal, μ, i.e., $\mu_{ph} = \mu - \mu_d$. The σ^2_{temp} versus μ_{pix_ph} curve is called the photon-transfer curve. This work refers to plots that contain this curve as "PTC plots".

In the dark and in low-light conditions, σ_{RN} is the dominant source of σ_{temp}, where the contribution of σ_{d_SN} in present days CIS is significant only at high temperatures with typical integration times. The contribution of σ_{ph_SN} to σ_{temp} increases with illumination until it becomes the dominant source of temporal noise. The region where σ_{RN} is the dominant source of σ_{temp} is marked as "RN" in **Figure 4** (c), and the "shot noise limited" region is marked as "SN" in the same figure.

Variance of noise sources with Poisson distribution equals the mean signal [5]. Therefore,

$$\sigma^2_{ph\_SN}[(e^-)^2] = \mu_{ph\_SN}\,[e^-], \qquad (1)$$

where "SN" stands for shot noise. Since $\sigma_{ph\_SN}{}^2\ [(e^-)^2] = \sigma_{ph\_SN}{}^2\ [DN^2] / SG^2 = \mu_{ph\_SN}\ [e^-] = \mu_{ph\_SN}\ [DN] / SG$,

$$\sigma^2_{ph\_SN}[DN^2] = SG \cdot \mu_{ph\_SN}\,[DN]. \qquad (2)$$

This relationship implies that in the shot-noise limited region of the PTC curve, the slope equals the system gain.

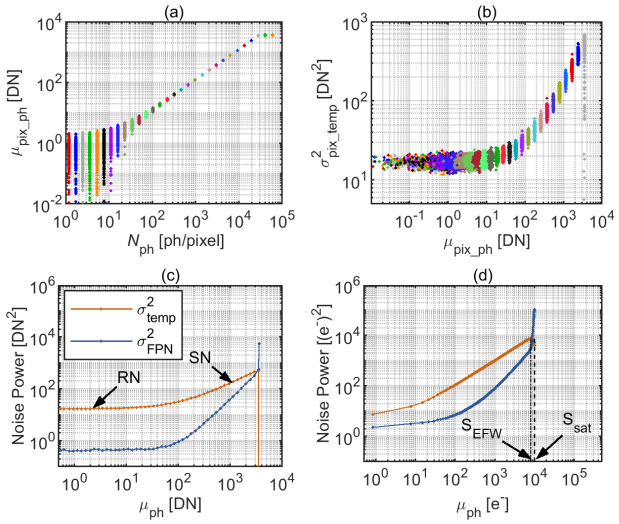

Figure 4. Plots (a) and (b) present simulation results under varied 530 nm illumination, where each color represents similar illumination level. Plots (c) and (d) are simulated and measured PTC plots, respectively, of an image sensor in SDR mode. The curves in (c) were calculated from the data points in plots (a) and (b). The marked regions in (c) and (d) are explained in the text.

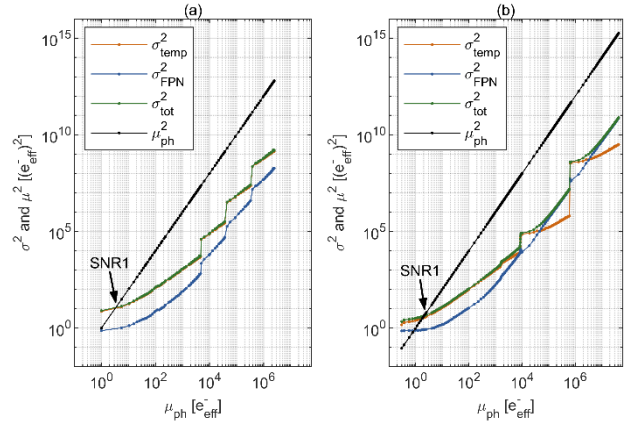

Figure 5. Measured PTC curves of image sensors in (a) 4-exposure HDR mode, and (b) overflow capacitor with second exposure HDR mode. SNR1 is signal level where $\mu_{ph} = \sigma_{tot}$, and $SNR_{tot} = 1 = 0$ dB.

The simulated PTC plot in **Figure 4** (c) is for an image sensor in SDR mode. **Figure 4** (d) presents a measured PTC plot of an image sensor in SDR mode. S_{EFW} is the signal level at the effective

full well (EFW) capacity, which is μ_{ph} at the peak of the PTC. S_{sat} is signal level at the maximum signal that the image sensor can reach with the configuration file that was used for the measurement [7], [8].

Figure 5 presents measured PTC plots of image sensors in (a) 4-exposure and (b) LOFIC and second exposure HDR mode. Total noise power, σ^2_{tot}, is calculated as $\sigma^2_{tot} = \sigma^2_{temp} + \sigma^2_{FPN}$. SNR1 is the noise-equivalent signal level, i.e., signal level at which $\mu_{ph} = \sigma_{tot}$. The total signal-to-noise ratio (SNR), SNR_{tot}, which is calculated as $SNR_{tot} = 20 \cdot \log_{10}(\mu_{ph}/\sigma_{tot})$ equals 1 = 0 dB at SNR1.

PTC Test Block Diagram

Figure 6 presents a workflow diagram of the PTC test, and Table 1 and Table 2 present definitions and formulas of parameters that are included in this diagram. Input data are sets of images that are captured in the dark and under uniform illumination with varied exposures. Image data are processed to calculate raw parameters, i.e., mean signal and noise. Raw parameters are then used to produce PTC and SNR plots, and these plots can be analyzed to derive image sensor metrics, such as SNR1, saturation level, and DR, and to convert raw parameters from DN to charge units [7], [8].

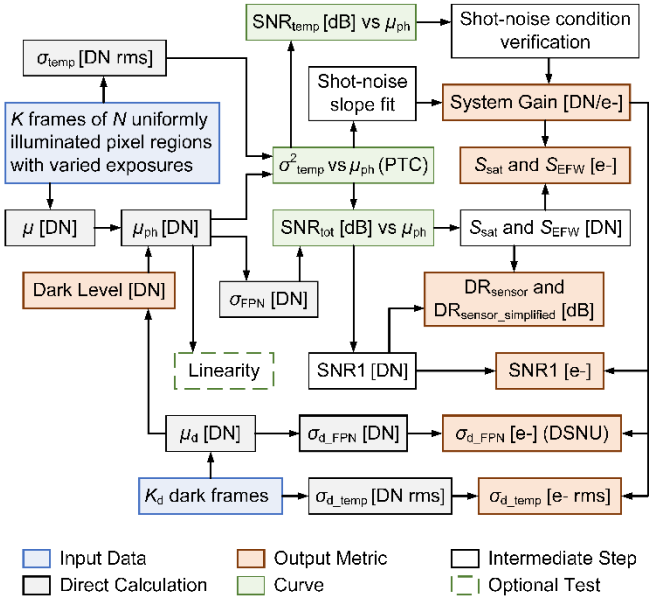

Figure 6. *Workflow diagram of the PTC test.*

Table 1. Parameters in the PTC workflow diagram

Parameter	Definition
μ, μ_d, μ_{ph}	Mean Signal: Total, Dark, Photo
σ_{temp}, σ_{d_temp}	Temporal Noise: Total, Dark
σ_{FPN}, σ_{d_FPN}	FPN: Total, Dark
SNR_{temp}, SNR_{tot}	SNR: Temporal, Total
S_{sat}, S_{EFW}	Signal: Saturation, EFW
DSNU	Dark Signal Non-Uniformity

Table 2. SNR and DR formulas

Parameter	Formula
SNR_{temp}	$20 \cdot \log_{10}(\mu_{ph}/\sigma_{temp})$
SNR_{tot}	$20 \cdot \log_{10}(\mu_{ph}/\sigma_{tot})$
DR_{sensor}	$20 \cdot \log_{10}(S_{EFW}/SNR1)$
$DR_{sensor\_simplified}$	$20 \cdot \log_{10}(S_{sat}/SNR1)$

Legacy PTC Test Procedure

Figure 7 (a) shows a photo of a setup to collect data for PTC measurements, where a camera kit with the camera lens removed is placed in front of an output port of an integrating sphere. Exposure is varied, and image data in raw format from two or more frames are saved or processed in real time at each exposure. This setup follows one of the options that are described in the EMVA 1288 standard [1]. The effective F# is adjusted by changing the diameter of the output port aperture and the camera-aperture distance.

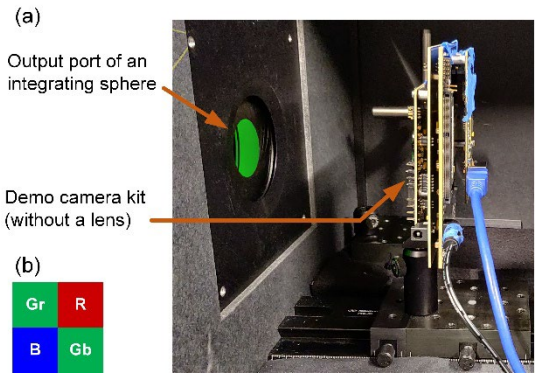

Figure 7. *(a) Setup for PTC measurements that follows legacy procedures. (b) A unit cell in Bayer pattern color image sensors.*

PTC in SDR Mode Example

This section discusses an example PTC test that was done in a setup like the one shown in **Figure 7** (a) with a color image sensor with 1 µm pixel size. The sensor was activated in SDR mode with 10-bit raw data format at T_j = 35 °C. The color filter array had the common Bayer pattern arrangement, where each 2×2 pixels unit cell includes two green, Gr and Gb, one red, R, and one blue, B, pixels, as shown in **Figure 7** (b).

The first image set was captured in the dark. Then, the image plane was illuminated with green light with constant intensity, and exposure was varied through change of T_{int}. At each exposure, two frames were saved from a region of 80×80 pixels at the center of the array, and there were 60 exposures in total. **Figure 8** (a) shows stitched images of all captured frames after separation to color channels. **Figure 8** (b) presents μ_{ph} versus T_{int} curves of all color channels, as calculated from the images in **Figure 8** (a). This measurement was done with a very low gain, to guarantee that photodiode saturation occurs at a signal level that is lower than the maximum digital signal, i.e., 1023 DN, because one of the goals was to derive the true full-well capacity of the photodiode. μ_d was 42 DN in this example. **Figure 8** (b) shows that only Gr and Gb pixels reach saturation, and that μ_{ph} < 500 DN at saturation.

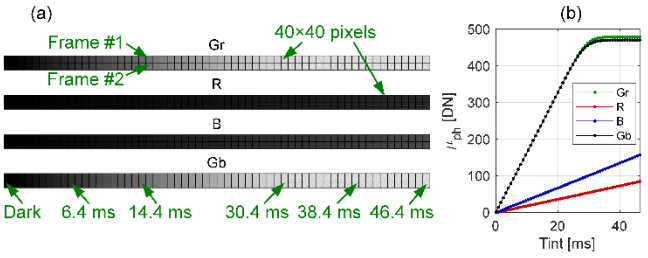

Figure 8. *(a) Stitched images of the four color-channels with two frames per exposure and 60 exposures in total. (b) μ_{ph} versus T_{int} curves as calculated from this image set. The sensitivity of the green channels is higher because the test was done with green light.*

The "Two-Frame" method and the "Per-Pixel" calculation are common approaches to calculate σ_{temp}. Both rely on the assumptions that: (a) the pixel signal is linear, (b) most pixels are rather similar, and (c) σ_{pix_temp} is uncorrelated in time and space.

The "Two-Frame" method is based on calculation of the standard deviation of the subtracted image. There are several versions to this approach, and (3) presents the one that is included in the EMVA 1288 standard Rel4.0 [1].

$$\sigma^2_{temp\_2f} = \frac{1}{2IJ}\sum_{j=1}^{J}\sum_{i=1}^{I}[S(i,j,1) - S(i,j,2)]^2 - \frac{1}{2}\big(\mu(0) - \mu(1)\big)^2, \quad (3)$$

where σ_{temp_2f} is σ_{temp} according to the "Two-Frame" method, I and J are the number of rows and columns, respectively, $S(i, j, k)$ is the signal of the pixel at location (i, j) in frame k, and $\mu(k)$ is the mean signal value of all pixels in the selected region in frame k. This approach is simple to implement and sufficiently accurate. The "Per-Pixel" calculation, which is the approach used in the IEEE P2020 Noise standard [7], incorporates two calculation steps. At first σ_{temp} is calculated per pixel, as shown in (4). Then the results are used to calculate σ_{temp} of the selected region, as shown in (5):

$$\sigma^2_{temp}(i,j) = \frac{1}{K-1}\sum_{k=1}^{K}[S(i,j,k) - \mu(i,j)]^2, \quad (4)$$

$$\sigma^2_{temp} = \frac{1}{IJ}\sum_{j=1}^{J}\sum_{i=1}^{I}\sigma^2_{temp}(i,j), \quad (5)$$

where K is the total number of frames. With the "Per-Pixel" approach, there is no restriction on the number of frames, and direct calculation of the distribution of σ_{pix_temp} is possible.

Figure 9 (a) presents PTC of the Gr channel as obtained from analysis of the images in **Figure 8** (a) using the "Two-Frame" method and the "Per-Pixel" calculation. Results show that the difference between the two approaches is negligible. Signal level at the peak of the PTC, which corresponds to full-well capacity [5], is 380.2 DN. The slope of the curve in mean signal range of 15-85% saturation level, which is marked with dashed lines, can be used to calculate the SG after verification that the region is shot noise limited. Verification is required by the IEEE P2020 Noise standard because there can be situations in which the PTC exhibits high linearity in the proper signal range although shot noise is not the dominant source of temporal noise. In these situations, the slope of the linear fit of the curve is not the SG.

If a signal range is shot-noise limited, the slope of the linear fit of the SNR_{temp} versus $\log10(\mu_{ph})$ curve is, ideally, 10 dB/decade. This value is obtained by combining (2) and the SNR_{temp} expression in Table 2 in a shot-noise limited region, as follows:

$$SNR_{temp\_SN} = 10 \cdot \log_{10}\left(\frac{\mu_{ph\_SN}\,[DN]}{SG}\right). \quad (6)$$

In practice, some tolerance is needed because of non-idealities. The slope of the fit line in **Figure 9** (b) is 10.2 dB/decade, which is sufficiently close. This confirms that the region is shot-noise limited, and the slope of the PTC in **Figure 9** (a) is the SG. Therefore, SG = 0.066 DN/ e^-, and the FWC is 380.2 [DN] / 0.066 [DN/e-] = 5.8 ke^-.

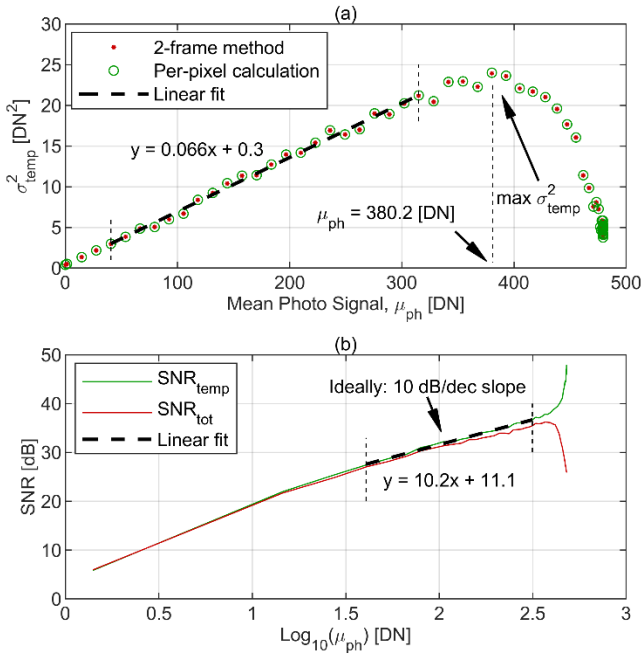

Figure 9. *(a) PTC as calculated with the "two-frame" and the "per-pixel" approaches. The parameters that were derived to calculate FWC and SG are explained in the text. (b) Verification that the selected signal range is shot noise limited.*

PTC in High Dynamic Range Mode

In HDR mode, variation of exposure can only be based on change of illumination because integration time sweep is either impossible or impractical. The PTC test setup that is described in the IEEE P2020 Noise standard is based on a transmissive back-illuminated chart. This setup is advantageous for test time reduction because it allows to collect data from multiple regions on the image plane simultaneously. However, it also has challenges since veiling glare and reflection artifacts are more pronounced when some portions of the scene are very bright.

Setup Optimization

Figure 10 presents images of an ITUHDR 36-patch back illuminated chart [9] when (a) light could pass through the entire chart area and (b) all chart area, excluding the patches, is covered

with an opaque mask. Both images were captured with the same camera from the same position. The camera included a color automotive image sensor which was activated in 3-exposure (3-EXP) HDR mode.

The ratio between transmission of the most transmissive to the least transmissive patch was greater than 150 dB, and DR_{sensor} with the configuration that was used for image capture was about 115 dB. Therefore, one would expect to cover the entire DR of the image sensor in a single frame. To calculate signal range in each image, 32 uniformly illuminated regions with 30×30 pixels each were manually selected in each image; they are marked in red squares. Mean photo-signal was calculated for each region, and **Figure 10** (c) presents μ_{ph} of the B channel versus measured patch attenuation curves for the two images.

The curves in **Figure 10** (c) show that μ_{ph} is not proportional to patch attenuation. This is a result of veiling glare, which is caused by light that is reflected back and forth inside the camera body. Veiling glare can increase the signal level of the entire array or local areas of the array and consequently violate any linear relationship between scene and image plane illumination [10]. Signal level of the two most transmissive patches in the image is saturation level, where $S_{sat} \approx$ 1E6 DN. Without a mask, minimum μ_{ph} is ≈ 1E3 DN, and the calculated $S_{sat}/\min(\mu_{ph})$ ratio is 57 dB. With a mask, minimum μ_{ph} is ≈ 60 DN, and the calculated $S_{sat}/\min(\mu_{ph})$ ratio is 84 dB. Although this value is smaller than the sensor DR, the 27 dB improvement is significant. A higher signal range allows to cover the entire sensor DR with a smaller number of exposures and, thus, to reduce test time. For this reason, veiling glare mitigation in setups that use a transmissive test chart is essential.

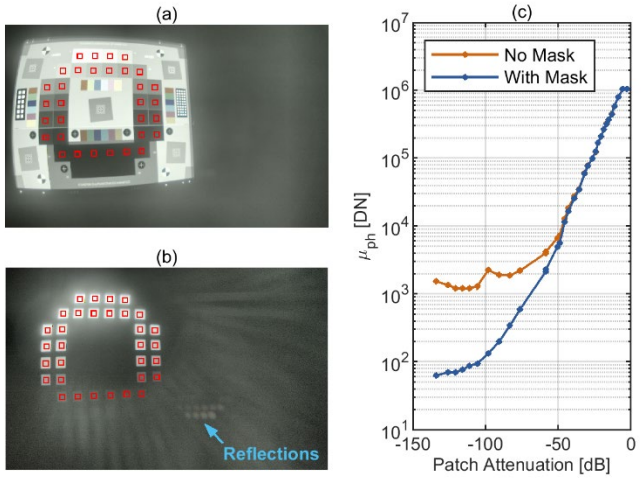

Figure 10. *Images of a transmissive back-illuminated test chart as captured (a) without and (b) with a mask. The red squares show the regions that were selected for calculation of μ_{ph}. (c) μ_{ph} versus measured patch attenuation curves of the images in (a) and (b).*

Ghost artifacts from reflections of the brightest patches can be observed in the photo in **Figure 10** (b). The user should position the camera to direct these reflections outside the chart region in the image as they can interfere with patch uniformity, which can have a negative effect on the accuracy of results and, especially, σ_{FPN}.

Example Results

Figure 11 presents results from a measurement that was done with a demo camera that included a color automotive image sensor in overflow with second exposure HDR mode. The image sensor was heated to achieve T_j = 105 °C. Two exposure conditions were needed to cover the entire sensor DR in this setup. Exposure was varied by changing the power of the LED panel behind the chart. **Figure 11** (a) and (b) present cropped single-frame images that were captured when the LED power was set to 0.4% and 100%, respectively. 30 frames were saved at each exposure, and the red rectangles mark the 32 pixel-regions with 26×36 pixels each that were used to calculate signal and noise parameters.

The two image sets were analyzed according to the procedure that is described in [8], and **Figure 11** (c) presents SNR_{temp} and SNR_{tot} curves. While SNR_{temp} does not drop below 30 dB for μ_{ph} > 1E3 DN, there is a sudden drop in SNR_{tot} in the data point that is pointed by arrow "2". Since SNR_{temp} is high at this signal level, σ_{temp} is low, hence, the drop in SNR_{tot} indicates a sudden increase in σ_{FPN}. To assess correlation between these results and end-user image quality, **Figure 11** (d) shows the region in an image from the 100% LED power image that includes the patches which correspond to data points "1" to "4" in **Figure 11** (c). The significant amount of granularity of patch "2", indicative of the hypothesized σ_{FPN}, can be observed, and it is obvious when the patch is compared to other patches and, specifically, patch "1", because its μ_{ph} is the closest to that of patch "2" among the four patches.

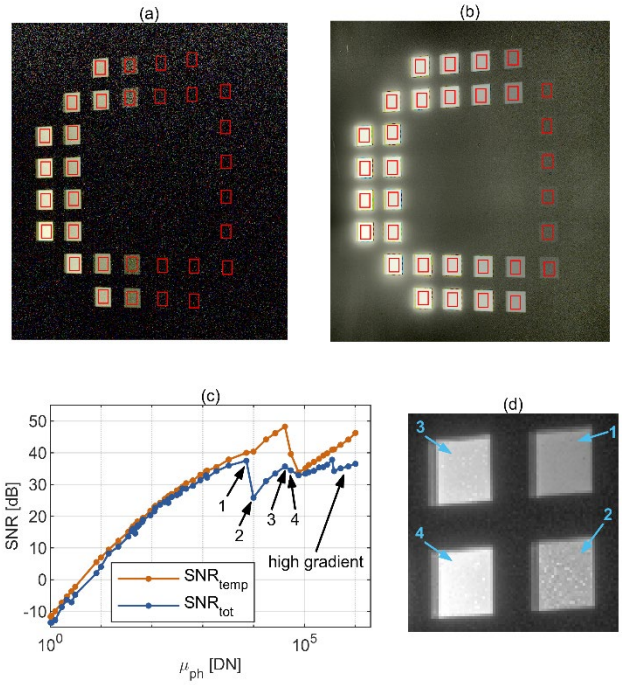

Figure 11. *Chart-based PTC measurement of an automotive image sensor in HDR mode with T_j = 105 °C. The images in (a) and (b) were captured when the LED panel power was set to 0.4% and 100%, respectively. The red rectangles are the regions that were selected for data analysis. (c) SNR_{temp} and SNR_{tot} curves of this measurement. (d) The patches that correspond to data points 1-4 in (c).*

The drop in SNR_{tot} in the last four data points of the curve is a measurement artifact that is caused by strong illumination gradient at the edge of the image, where the four most transmissive patches are located. The gradient increases non-uniformity and adds to σ_{FPN}. A method for evaluation of the contribution of illumination gradients to σ_{FPN} is not defined in current standards.

Linearity

The straightforward approach for evaluation of linearity of a light detector is based on a linear regression of its mean photo signal as a function of the irradiance of a calibrated light source with a steady spectral power distribution (SPD). The EMVA 1288 standard uses this approach. In this standard, evaluation is done in the 5-95% signal range to exclude signal levels that are too close to dark level and saturation, where a higher deviation from linearity is expected.

Figure 12 presents example results from a linearity test that was conducted with an image sensor in SDR mode with 12-bit raw data format according to the procedure in the EMVA 1288 standard. Green light in a setup like the one in **Figure 7** had a central wavelength of 543 nm and 35 nm full-width half-maximum (FWHM). μ_{ph} was calculated from data of 1000×1000 pixels at the center of the array, where light level was varied 50 times, and 20 frames were processed at each exposure. Calculation of fit line coefficients, relative deviation, δ, and linearity error (LE) followed the procedure that is described in section 6.9 of the EMVA 1288 standard [1].

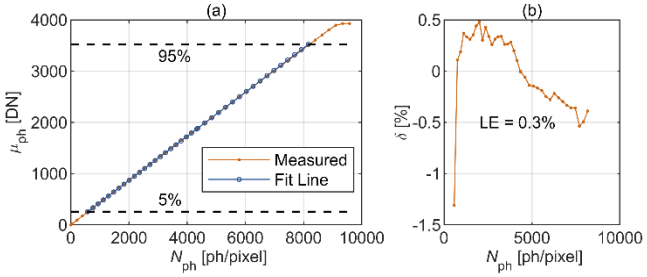

Figure 12. *Linearity measurement of an image sensor in SDR mode according to the EMVA 1288 standard. (a) Measured μ_{ph} values and a linear fit line. (b) The relative deviation curve and linearity error (LE).*

This method for evaluation of linearity can be challenging to implement with image sensors in HDR mode, mainly because of the requirement for the light source to have a steady narrow-band SPD across a signal range that covers the full DR of the HDR sensor. The approach that is taken with image sensors in HDR mode is based on the inter-channel response [11]. A stable SPD is required, however, there is no need to measure source irradiance.

In the ideal case, when the response of all color channels is perfectly linear, the ratio between μ_{ph} of one color-channel, μ_{ph_1}, and μ_{ph} of another one, μ_{ph_2}, must be constant in the entire signal range, excluding regions that are too close to dark and saturation levels, i.e., $\mu_{ph\_1}(n)/\mu_{ph\_2}(n) = C_{12}$, where n is a data point index and C_{12} is a constant. By applying log10 on both sides of this equation for data points n and n+1, the following equations are obtained: $\log_{10}(\mu_{ph\_1}(n))-\log_{10}(\mu_{ph\_2}(n)) = \log_{10}(\mu_{ph\_1}(n+1)) - \log_{10}(\mu_{ph\_2}(n+1)) = \log_{10}(C_{12})$. Rearrangement of the elements on both sides of the equation gives:

$$\frac{\log_{10}(\mu_{ph\_1}(n+1)) - \log_{10}(\mu_{ph\_1}(n))}{\log_{10}(\mu_{ph\_2}(n+1)) - \log_{10}(\mu_{ph\_2}(n))} = 1. \qquad (7)$$

The left side of this equation is a one-sided derivative of the $\log_{10}(\mu_{ph\_1})$ versus $\log_{10}(\mu_{ph\_2})$ curve, and its right side shows that a deviation of the derivative from "1" indicates on deviation from linearity. The same method can be applied to a monochrome image sensor with use of attenuation filters.

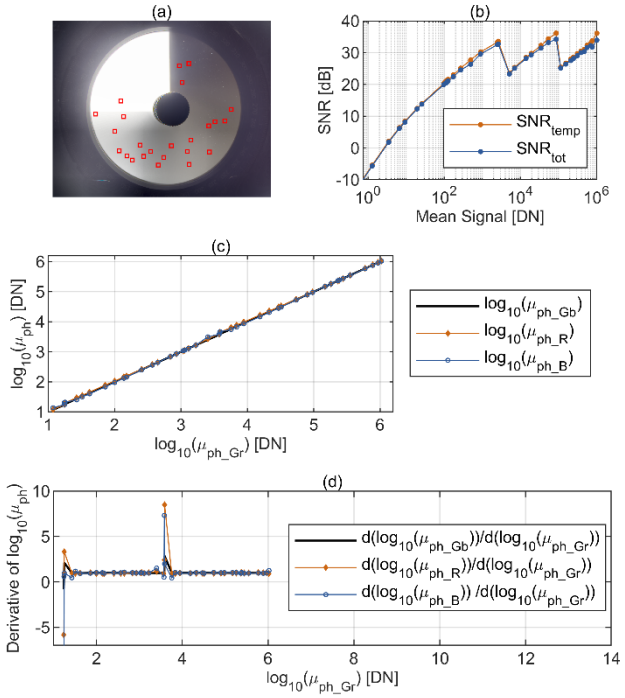

Figure 13. *Linearity in HDR mode: (a) An image of a back-illuminated variable neutral density filter with pixel regions that were selected for data analysis. (b) SNR curves of the same image sensor with the same configuration file. (c) Log10 of μ_{ph_R}, μ_{ph_Gb}, and μ_{ph_B} versus log10 of μ_{ph_Gr}. (d) Derivatives of the curves in plot (c).*

Figure 13 (a) presents an image of a variable neutral density filter that was placed in front of the output port of an integrating sphere. This filter is a glass substrate with metallic coating with varied optical density. The image was captured with a color automotive image sensor in 3-EXP HDR mode. Two light levels were needed to cover the entire DR of the image sensor. To ensure that the illuminant SPD cannot change with light level, light level was changed through control of the opening of a variable width slot which was located at the input port of the integrating sphere. The red rectangles are 24 regions with 20×20 pixels each that were manually selected for data analysis.

Figure 13 (b) shows the SNR curves of the same image senor as measured when it was activated with the exact same configuration file. **Figure 13** (c) presents $\log_{10}(\mu_{ph})$ curves of the R, Gb, and B color channels versus $\log_{10}(\mu_{ph})$ of the Gr channel, and **Figure 13** (d) presents the derivatives of these curves. In **Figure 13** (d), there is a small deviation from "1" close to the origin and a larger one when $\mu_{ph\_Gr} \approx$ 5E3 DN. The former may be a measurement artifact at the first data point or a real deviation from linearity at low signal levels. The latter occurs at a signal level which, according to **Figure 13** (b), is the first transition of the 3-EXP HDR response. This indicates an imperfection in the algorithm that was used to construct the linearized HDR response in this example. The imperfection, which was detected by the derivative, is causing deviation from linearity at the first transition.

Conclusion

This work discussed differences in approaches to implement the photon-transfer curve test between legacy procedures which were optimized for image sensors in SDR mode and the procedure

in the IEEE P2020 Noise standard, which is developed for automotive cameras where image sensors are predominantly operated in HDR mode. The IEEE P2020 Noise standard considers the important factor of best trade-off between measurement accuracy, test practicality, and test time economy.

Acknowledgement

The authors thank Sergey Velichko, Yvonne Lee, Darryl Perks, Barry Vanhoff, Rujul Desai, and Shaheen Amanullah for advice and data. They also thank the IEEE P2020 Working Group participants who assisted with the development of the Noise standard.

References

[1] European Machine Vision Association,, "EMVA Standard 1288 - Standard for Characterization of Image Sensors and Cameras, Release 4.0 Linear, 2021".

[2] D. X. D. Yang and A. El Gamal, "Comparative analysis of SNR for image sensors with enhanced dynamic range," in *Proc. SPIE*, 1999.

[3] A. Nana, A. Satoru, M. Koichi and S. Shigetoshi, "Optimum Design of Conversion Gain and Full Well Capacity in CMOS Image Sensor With Lateral Overflow Integration Capacitor," *IEEE Transactions on Electron Devices,* vol. 56, no. 11, pp. 2429-2435, 2009.

[4] I. Takayanagi and R. Kuroda, "HDR CMOS Image Sensors for Automotive Applications," *IEEE Transactions on Electron Devices,* vol. 69, no. 6, pp. 2815-2823, 2022.

[5] J. R. Janesick, Photon Transfer DN to Lambda, SPIE Press, 2007.

[6] A. El Gamal and H. Eltoukhy, "CMOS image sensors," *IEEE Circuits and Devices Magazine,* vol. 21, pp. 6-20, 2005.

[7] *IEEE P2020/D3 Draft Standard for Automotive System Image Quality,* 2022.

[8] O. Skorka and P. Romanczyk, "A review of IEEE P2020 noise metrics," in *IS&T International Symposium on Electronic Imaging: Autonomous Vehicles and Machines*, 2022.

[9] Imatest, "Imatest 36-Patch Dynamic Range Test Charts," [Online]. Available: https://www.imatest.com/product/dynamic-range-test-charts/. [Accessed 2024].

[10] J. J. McCann and A. Rizzi, "Camera and visual veiling glare in HDR images," *Journal of the Society for Information Display,* pp. 721-730, 2007.

[11] O. Skorka, B. Vanhoff, R. Desai and R. Ispasoiu, "Method for Evaluation of Linearity of Image Sensors in High Dynamic Range Mode," *IEEE Sensors Journal,* vol. 23, no. 11, pp. 11582-11590, 2023.